Prediction of PA12 melt viscosity in Laser Sintering by a Time and Temperature dependent rheological model

M.Sc. C. Mielicki[1], Dipl.-Ing. A. Wegner[2], Dipl.-Ing. B. Gronhoff[1],
Prof. Dr.-Ing. J. Wortberg[1], Prof. Dr.-Ing. habil. G. Witt[2]
University of Duisburg-Essen, Institute of Product Engineering:
[1]Engineering Design and Plastics Machinery
[2]Manufacturing Technology, Duisburg, Germany

Zusammenfassung

Ein auf Basis von Prozessdaten kalibriertes Viskositätsmodell wird vorgeschlagen und zur Vorhersage der Viskosität einer Polyamid 12 (PA12) Kunststoffschmelze als Funktion von Zeit, Temperatur und Schergeschwindigkeit angewandt.

Im ersten Schritt wurde das Viskositätsmodell aus experimentellen Daten abgeleitet. Es beruht hauptsächlich auf dem drei-parametrigen Ansatz von Carreau, wobei zwei zusätzliche Verschiebungsfaktoren eingesetzt werden. Die Temperaturabhängigkeit der Viskosität wird mithilfe des Verschiebungsfaktors a_T von Arrhenius berücksichtigt. Ein weiterer Verschiebungsfaktor a_{SC} (Structural Change) wird eingeführt, der die Strukturänderung von PA12 als Folge der Prozessbedingungen beim Lasersintern beschreibt. Beobachtet wurde die Strukturänderung in Form einer signifikanten Viskositätserhöhung. Es wurde geschlussfolgert, dass diese Viskositätserhöhung auf einen Molmassenaufbau zurückzuführen ist und als Nachkondensation verstanden werden kann. Abhängig von den Zeit- und Temperaturbedingungen wurde festgestellt, dass die Viskosität als Folge des Molmassenaufbaus exponentiell gegen eine irreversible Grenze strebt. Die Geschwindigkeit dieser Nachkondensation ist zeit- und temperaturabhängig. Es wird angenommen, dass die Pulverbetttemperatur einen Molmassenaufbau verursacht und es damit zur Kettenverlängerung kommt. Dieser fortschreitende Prozess der zunehmenden Kettenlängen setzt molekulare Beweglichkeit herab und unterbindet die weitere Nachkondensation. Der Verschiebungsfaktor a_{SC} drückt diese physikalisch-chemische Modellvorstellung aus und beinhaltet zwei zusätzliche Parameter. Der Parameter $a_{SC,UL}$ entspricht der oberen Viskositätsgrenze, wohingegen k_0 die Strukturänderungsrate angibt. Es wurde weiterhin festgestellt, dass es folglich nützlich ist zwischen einer Fließaktivierungsenergie und einer Strukturänderungsaktivierungsenergie für die Berechnung von a_T und a_{SC} zu unterscheiden.

Die Optimierung der Modellparameter erfolgte mithilfe eines genetischen Algorithmus. Zwischen berechneten und gemessenen Viskositäten wurde eine gute Übereinstimmung gefunden, so dass das Viskositätsmodell in der Lage ist die Viskosität einer PA12 Kunststoffschmelze als Folge eines kombinierten Lasersinter Zeit- und Temperatureinflusses vorherzusagen.

Das Modell wurde im zweiten Schritt angewandt, um die Viskosität während des Lasersinter-Prozesses in Abhängigkeit von der Energiedichte zu berechnen. Hierzu wurden Prozessdaten, wie Schmelzetemperatur und Belichtungszeit benutzt, die mithilfe einer High-Speed Thermografiekamera on-line gemessen wurden. Abschließend wurde der Einfluss der Strukturänderung auf das Viskositätsniveau im Prozess aufgezeigt.

Abstract

A rheological model was derived from experimental data and has been proposed to predict the viscosity of a Polyamide 12 (PA12) melt as a function of time, temperature and shear rate.

*In a first step, the rheological model was derived that is mainly based on the well-known three parameter Carreau model. In addition, two shift factors were introduced to the model. The shift factor a_T by Arrhenius considers the temperature dependence of the viscosity. A second shift factor a_{SC} (SC: **S**tructural **C**hange) is proposed. This factor describes the structural change that was observed as a significant viscosity build-up, concluded as molar mass build-up and understood as post condensation of PA12 at LS process conditions. In fact, at temperatures and times investigated, the effect on viscosity was found to be of exponential, limited and irreversible growth behaviour. The rate of post condensation is time and temperature dependent. It is assumed that powder bed temperature leads to molar mass build-up of PA12 because of consumption of molecular chains into molecular chain extension. Moreover, the progressing formation of extended molecular chains however decreases molecular movement and finally freezes post condensation. This physiochemical model assumption is expressed in the form of the structural change shift factor a_{SC} that introduces two additional parameters to the rheological model. The parameter $a_{SC,UL}$ corresponds to the upper limit whereas k_0 is correlated to the rate of structural change. Furthermore, it was found to be suitable to use individual activation energies for a_T and a_{SC} calculation, i.e. to differentiate between flow activation and structural change activation energy. Based on experimental data, rheological model parameters were optimised using a genetic algorithm. The comparison of predicted viscosity with experimental data was found to be in good agreement. Hence, the rheological model is suitable to predict the viscosity of a PA12 as result of a combined LS process time and temperature influences.*

In a second step, the model was applied in order to calculate the viscosity during the laser sintering process as a function of energy density, by using data for the melt temperature and laser exposure time which were measured on-line with a high-speed-thermal imaging system. Moreover, the effect of structural change on the viscosity of PA12 is shown with respect to LS process time and temperature.

1. Introduction

Increasing competition, decreasing product life cycles, the wish for customized products and a shortage of resources cause the need for innovative manufacturing techniques for small series production [1]. Going beyond the stage of Rapid Prototyping on to Rapid Manufacturing, Additive Manufacturing offers possibilities for small series production of customised products and an increased freedom of design, due to the lack of tools [2]. The laser sintering (LS) of plastic parts is, aside from beam melting of metal parts, one of only two AM-processes which have the capability to be used for Rapid Manufacturing in the near future [3]. In laser sintering, parts are built up layer by layer using layer thicknesses between 0.06 and 0.18 mm. The machine produces the parts by repeating three stages for each layer: Firstly, the platform descends by the thickness of one layer. Secondly, powder is spread across the build platform by a levelling roller or coater and preheated to a temperature close to the material melting point by a radiant heater. Finally, a CO2-laser beam melts the powder by tracing the actual cross section line after line, using a scanner system. These steps are repeated until the parts are completed [4]. In comparison to conventional plastics processing techniques, like injection moulding or extrusion, laser sintered parts are manufactured at unpressurised processing conditions. The driving force in LS is the temperature increase in the powder bed caused by laser exposure. Hence, the resulting part properties strongly depend on the interaction of energy input, the melt temperature and the melt viscosity.

With respect to material properties, viscosity is the most significant property that affects processes and parts in laser sintering. The evaluation of flow properties is therefore reasonable because of the fact that coalescence of adjacent polymer particles during the unpressurised LS manufacturing procedure is strongly dependent on viscous flow properties [5]. Thus, viscosity determines the sintering velocity, the resistance towards melt formation and the bonding strength of sintered layers as well as the part porosity. Moreover, the viscosity is directly related to the structure of the molten polymer. On the one hand, a low melt viscosity can be achieved for high melt temperatures resulting from high laser powers [6] leading also to a high degree of particle melt [7]. On the other hand, the melt viscosity is also a value specific to the particular material used, which is influenced by the chosen powder type and its additives. For laser sintering, the materials melt viscosity is modified to be very low. In laser sintering processes, the utilisation of material weight for part production

is far less than 30%, e.g. in comparison to injection moulding [8]. As a result, a huge amount of powder that was stored at process conditions remains un-sintered from each build process. Due to the high material cost, which might be ten times higher in comparison to thermoplastic materials for injection moulding, recycled material should be reused in order to sustain economic and resource efficiency. However, un-sintered powder material undergoes an aging process caused by LS processing time and temperature. The result of material aging due to process conditions has already been reported, especially for PA12 powder, as a significant change in viscosity or melt flow/volume rate. The change in flow properties was concluded to be a powder degradation process [8], a polycondensation process [9] or a post curing or polymerization process with simultaneously occurring chain degradation [10]. Although structural change was found, the magnitude of its influence on process and part properties is still unknown. As a result, material quality control as well as process control cannot be established successfully so that part properties cannot be guaranteed. In particular, these changes in properties, i.e. viscosity and in addition process deviations prevent the LS technology from manufacturing of quality assured parts in a series production. A quality assured series production is only successful as soon as material property deviations and process related material property changes are known and controllable by means of process understanding [11]. Therefore, process related viscosity changes are in the focus of this investigation.

Nowadays, recycled powder is refreshed with virgin powder in order to keep the materials quality on a sufficient level to produce parts without orange peel [12] or reduced mechanical properties [13]. Typical refresh strategies for PA12 powders use 30 to 50 % virgin powder. However, this refreshing process results in a powder mixture without defined properties, not allowing for a quality assurance of the powder material.

2. State of technology

Correlations between material aging, material properties and part properties have been analysed in several publications. In 2001, Choren presented in [14] some first analyses. He aged powder artificially by performing build processes with a duration of 24 h in order to analyse the correlation between powder age and process control, for mechanical properties parallel to the building platform as well as the part geometrical accuracy. In [15], Sauer performed similar analyses, but found partially contrary results while using the same machine type and material. These results were proven by results given by Gornet [16, 17], who found similar tendencies for part properties. Additionally, Gornet analysed the surface quality of laser sintered parts as a function of powder age and found “orange peel”, which is a typical effect of material aging in laser sintering, after six process cycles, while mechanical properties would not have descended before further process cycles. In further analyses, he used MFR- and DSC-measurements to determine material changes and proved that melt flow rates can be used to measure material aging. Similar analyses in [18] also show a significant increase in viscosity for aged material, while using a rotational viscosimeter as a measuring system. Additionally, Seul, for the first time, correlates material aging with an increase in molecular weight and with post polymerisation effects. In addition to an increase of melting temperature which can be also found in [18], Seul measured a rising crystallisation temperature for increasing powder age. Wegner, in [13] analysed part density and mechanical properties of PA12 parts as a function of material aging, also considering different parameter sets and part orientations. He showed that an increasing material age always leads to a decrease of part density and mechanical properties especially in z-direction. Additionally, he found that this effect is nearly negligible up to aging times of 25 h, when using high energy densities above 0.33 J/mm³. However, when using lower energy densities, this effect already occurs before an aging time of 25 h, resulting in a significant reduction of mechanical properties in z-direction, while no reduction of surface quality can be observed for that aging time. This is in contrast to results found in other publications, where surface quality is named to be the most sensitive property for material aging. However, in all other publications mechanical properties in z-direction were not considered.

In [10], powder samples were stored in an oven, performing a model experiment in order to analyse influences on melting and crystallisation temperature. Results show that the processing window for laser sintering process grows for an increase of material age. Reasons for that were found in an ascent of melting temperature, while crystallisation temperature decreases at the same time due to post polymerisation. Drummer proves that besides MFR- and MVR-measurement, viscosity number is also adequate to monitor powder

quality.

With the aim of identifying more detailed correlations for material aging, in [19] , Pham aged Polyamide powder in an oven at temperatures between 100 and 180 °C using storage times between 10 and 200 h. Results showed that MFR-values are more sensitive to aging effects than all temperature values measured by a DSC. He found the main changes of the MFR-value for temperatures over 150 °C within the first 20 h of aging time. Additionally, Pham developed a performance measurement system in order to study surface quality of laser sintered parts by evaluating the surface quality of different geometries. He used this system in [20] to achieve a sufficient surface quality by adjusting the process parameters when using a poor powder quality. Based on these results, Dotchev qualified MFR-measurement for the characterisation of powder quality, [8]. On the one hand, he performed aging experiments using an oven in order to determine fundamental aging mechanisms. On the other hand he analysed the dependency of powder quality on the build space position for different machines and different build processes. He found that powder at the edges and at the top of the build envelope, as well as powder from short processes, shows the lowest deterioration and the highest MFR-values, while powder in the build space centre and of long build processes is significantly deteriorated. Further analyses on the mixture of different powder qualities show that a poor powder quality will dominate the quality of the mixture. Powders with very low MFR-values require high refreshing rates in order to achieve a sufficient material quality. Therefore, an optimised refreshing and segregation strategy using MFR-measurements can significantly reduce consumption of powder and can guarantee powder quality in laser sintering.

In addition to the state of technology presented before, which determines correlations between part properties and material aging, several attempts were performed to analyse the laser-powder interaction, while measuring process temperatures. However, sometimes restrictions regarding the informative value of the measurements resulted from the chosen experimental setup. Keller measured the melt temperature just after exposure to laser light as a function of different parameter sets and densities of energy [21]. The results showed a linear correlation between the melt temperature and density of energy. Nöken [22] analysed surface temperatures and the melt temperature when processing polystyrene. He measured the temperatures through the machine viewing window at an observation angle of 60° using a medium wave thermal imaging system. Additionally, the viewing window had a transmission rate of only 25 %. Due to that test setup, the measured values will significantly deviate from the real temperatures on the powder bed surface. This test setup was improved in [23] by replacing the original viewing window with an assembly containing a zinc-selenide window, with a high transmission rate. However, the large viewing angle was kept in this solution. Fischer [24] and Kosolov [25] analysed the temperature in the laser focus using

thermal imaging while processing titanium, while Wiria [26] did similar analyses for polyvinyl alcohol. At the catholic university of Leuven, a feedback control system was developed in order to monitor melt temperatures and melt pool size in beam melting using a CMOS-camera [27, 28]. Another solution for temperature monitoring in laser sintering and laser beam melting is presented in [29]. It uses a two-wavelength pyrometer for determining the temperature and a high-speed CCD-camera to measure the temperature distribution in the laser focus by measuring spatial brightness. However, the paper only contains measured data for Titanium. Gao [30] used a thermal imaging system for temperature measurements in combination with a dual wavelength pyrometer for system calibration. However, the paper only provides little information on the experiments. Another study to measure melt temperature is presented by Kumpaty in [31]. He used a pyrometer to measure the temperature during laser exposure. However, the pyrometer used within the setup has a spot size of 25 mm, allowing only for measurements of average temperatures, hence giving no information on the maximum temperature in the laser focus. Some of our own analyses to measure the melt temperature were presented in [6]. The experiments setup and the results described there are the basis for the measurement of melt temperatures in this paper while using an improved setup and a high-speed-thermal imaging systems.

Literature review shows, that there is only little detailed information on the melt viscosity of laser sintering materials as well as no correlations between process parameter settings, resulting melt temperatures during and after laser exposure and melt viscosity. Therefore, process related viscosity changes are in the focus of this investigation. Aim of the research is to establish a time and temperature dependent rheological model which should be applied to the laser sintering process in order to establish a correlation between energy input and melt viscosity by using results from thermal imaging measurements. These correlations will improve the understanding of the interaction of laser energy and powder material in laser sintering, by giving for the first time information on the melt viscosity during the laser sintering process.

3. Experimental

3.1. MVR measurements

Experimental data were obtained using melt flow indexer (MFI) equipment. Viscosity, shear stress and shear rate were calculated from melt volume rate (MVR) data [32]. In order to evaluate the change of viscosity with respect to time dependence as a result of process conditions, PA12 (PA2200, EOS) was systematically aged in a vacuum oven (Model: VT 6060 P-400, Thermo Scientific) that had been pre-heated to 174°C for 1 hour. At 174°C, the powder was inserted into the vacuum oven which was immediately evacuated for 400 sec. Afterwards, the oven was flooded with N_2 to provide inert gas atmosphere during aging. According to this procedure, PA12 powder with aging times of 1, 2.5, 5, 10, 20 and 120 hours was systematically obtained. MVR data were measured according to DIN EN ISO 1133 using an adopted capillary rheometer (Model: Galaxy V, Dynisco). Prior to the MVR measurements, powder samples had been dried in the vacuum oven under N_2 atmosphere at 90°C for 4h and cooled under N_2 atmosphere to ambient temperature. MVR were measured at three temperatures with three different loads to cover the temperature dependence within a shear rate range of approx. 1 – 1000 1/s (Table 1).

Table 1: Experimental set-up MVR measurements

Aging time	Temperature	Load
[h]	[°C]	[kg]
0	200/220/240	3.5/5/12.5
1	200/220/240	3.5/5/12.5
2.5	200/220/240	3.5/5/12.5
5	200/220/240	3.5/5/12.5
10	200/220/240	3.5/5/12.5
20	200/220/240	3.5/5/12.5
120	200/220/240	3.5/5/12.5

Every aging time, temperature and load combination was measured three times to study the range of viscosity variation. In total 189 measurements were carried out.

3.2. Thermal imaging

A high-speed thermal imaging system InfraTec Image IR 5300 was implemented into a DTM Sinterstation 2500 with High-Speed-Upgrade in order to measure the melt temperature during and after laser exposure as a function of different process parameters. This camera system has an optical resolution of 320 x 256 Pixels, a maximum temporal resolution of 3000 Hz using quad frame mode and a wavelength range from 2.5 – 5.5 µm. The camera is placed adjacent to the scanner head with an observation angle of 29°, allowing for the measurement of the melt temperature during laser exposure (figure 1). For this purpose, a telephoto lens with a focal distance of 100 mm and a 500 mm close up lens is used, resulting in an optical resolution of 0.147 mm at a distance of 490 mm, which is the ideal resolution for the laser focus diameter of 0.45 mm. Using that setup, the field of view is limited to a size of 11.8 by 9.4 mm. This only allows for measuring temperatures in single points or a small area of real parts. However, the aim of the research here is to determine the melt temperature and not the temperature distribution in bigger parts. To avoid potential damage of the thermal imaging system by the CO2-laser, a sapphire window is used, which cuts off all radiation above 6 µm, but has a very high transmission rate in the camera wavelength range. Specimens for the analysis were cuboids with a length of 25 mm. Five single points were evaluated for each layer, comparing two layers for each set of parameters. The measured data were used to determine the maximum temperature of the melt during laser exposure as well as the average melt temperature within the observed area ten seconds after laser exposure. Virgin EOS PA 2202 black powder was chosen for temperature measuring in order to increase emissivity in comparison to white PA 2200.

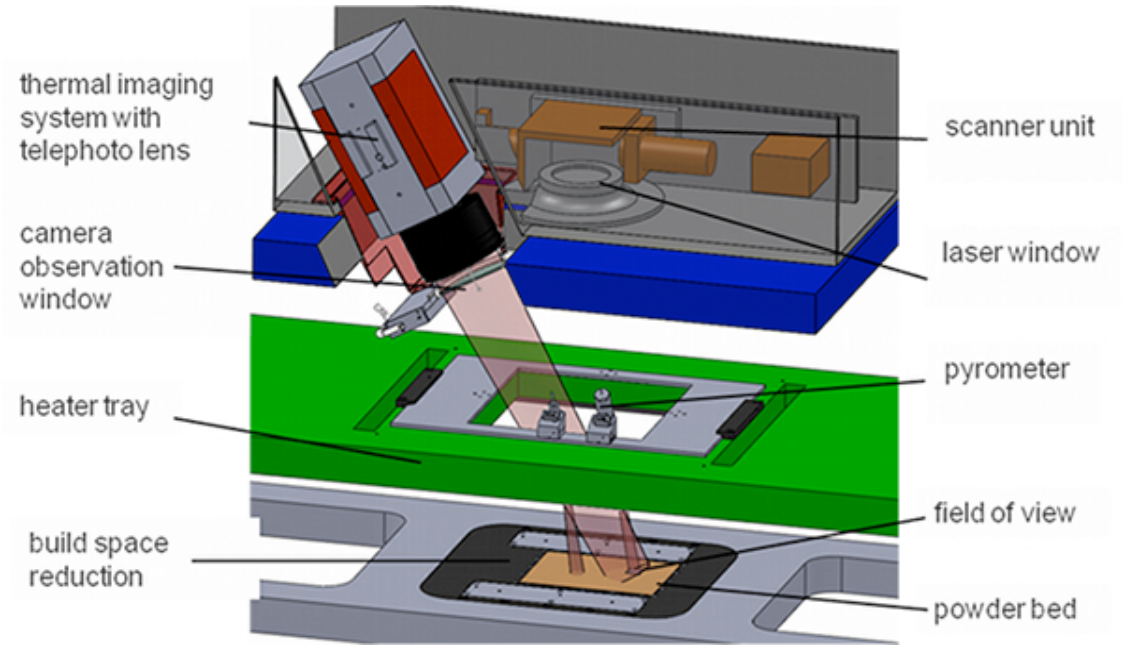

Figure 1: Experimental setup for the measuring of the melt temperature

DOE approach based on central composite design was used to establish an experimental design for measuring the melt temperature as a function of different process parameters. This design considers the five main influences in laser sintering and was also used to perform other analyses not presented here. Selected influencing factors were laser power, scan spacing, scan speed, powder bed temperature and layer thickness. The design results in a total of 36 different experimental points with very different parameter combinations having a margin of 0.016 J/mm² up to 0.050 J/mm² for area energy density. The lowest considered energy density is similar to the energy input used for 3D-systems machines, while the highest value is above the energy input of EOS' machines. The plan of experiments used is summarised in table 2. Within the results presented here, area energy density was used to establish correlations for the laser sintering process.

Table 2: Plan of experiments and measured data

	Laser power	Scan spacing	Scan speed	Powder bed temperature	Layer thickness	Area energy density	Max. melt temperature	Melt temp.10 s after exposure
EN	W	mm	m/s	W	mm	J/mm²	°C	°C
1	39	0.15	7.0	175	0.15	0.037	296.6	188.4
2	46	0.15	7.0	175	0.1	0.044	312.3	191.4
3	39	0.25	7.0	175	0.1	0.022	249.6	184.2
4	46	0.25	7.0	175	0.15	0.026	271.9	179.7
5	39	0.15	10.0	175	0.1	0.026	267.4	187.8
6	46	0.15	10.0	175	0.15	0.031	282.4	185.7
7	39	0.25	10.0	175	0.15	0.016	232.3	171.1

8	46	0.25	10.0	175	0.1	0.018	244.8	174.2
9	39	0.15	7.0	177	0.1	0.037	297.0	190.4
10	46	0.15	7.0	177	0.15	0.044	316.0	188.1
11	39	0.25	7.0	177	0.15	0.022	255.5	181.0
12	46	0.25	7.0	177	0.1	0.026	269.9	189.3
13	39	0.15	10.0	177	0.15	0.026	265.6	187.1
14	46	0.15	10.0	177	0.1	0.031	286.9	190.3
15	39	0.25	10.0	177	0.1	0.016	228.5	172.1
16	46	0.25	10.0	177	0.15	0.018	245.6	177.5
17	35.5	0.2	8.5	176	0.125	0.021	247.3	179.6
18	49.5	0.2	8.5	176	0.125	0.029	285.6	190.9
19	42.5	0.1	8.5	176	0.125	0.050	330.8	192.8
20	42.5	0.3	8.5	176	0.125	0.017	235.9	172.8
21	42.5	0.2	5.5	176	0.125	0.039	298.2	191.7
22	42.5	0.2	11.5	176	0.125	0.018	241.3	178.4
23	42.5	0.2	8.5	174	0.125	0.025	265.2	182.2
24	42.5	0.2	8.5	178	0.125	0.025	268.7	191.5
25	42.5	0.2	8.5	176	0.075	0.025	265.1	190.1
26	42.5	0.2	8.5	176	0.175	0.025	259.3	180.8
27	42.5	0.2	8.5	176	0.125	0.025	263.5	188.2
28	42.5	0.2	8.5	176	0.125	0.025	267.5	187.8
29	42.5	0.2	8.5	176	0.125	0.025	265.0	187.7
30	42.5	0.2	8.5	176	0.125	0.025	266.3	187.7
31	42.5	0.2	8.5	176	0.125	0.025	266.8	188.3
32	42.5	0.2	8.5	176	0.125	0.025	267.8	189.1
33	42.5	0.2	8.5	176	0.125	0.025	265.5	188.0
34	42.5	0.2	8.5	176	0.125	0.025	265.6	187.7
35	42.5	0.2	8.5	176	0.125	0.025	267.3	188.7
36	42.5	0.2	8.5	176	0.125	0.025	265.6	188.6

4. Results

4.1. MVR results

Melt volume rate of PA12 as function of aging time t_A at different temperatures is shown in figure 2 below.

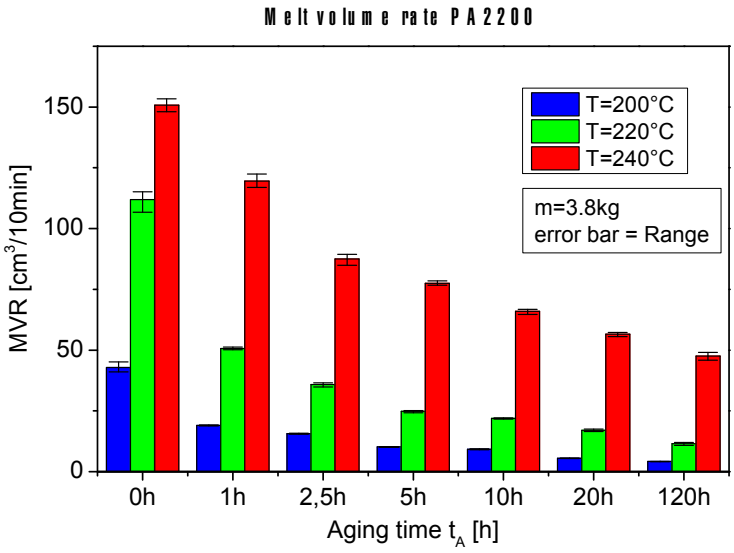

Figure 2: MVR of PA12 (m=3.8kg)

As it can be seen, the higher the temperature, the higher is the MVR. However, MVR strongly decreases as function of aging time or with rising aging time respectively. In comparison to the range of MVR variation at t_A=0h, the influence of rising aging time was found to be significant. Moreover, the range of MVR variation is relatively small and proves a good repeatability of measurement. At temperatures of 200 to 240°C, MVR drops continuously within the investigated time of aging. Furthermore, the influence of aging on MVR is higher at a lower temperature, i.e. a higher temperature can partially compensate powder aging. For example, MVR drops at a temperature of 240°C from 150.8cm^3/10min to 47.5cm^3/10min which is a factor of approx. 3.2. In contrast, MVR drops at a temperature of 200°C from 42.8cm^3/10min to 4.2cm^3/10min which is a factor of approx. 10.2.

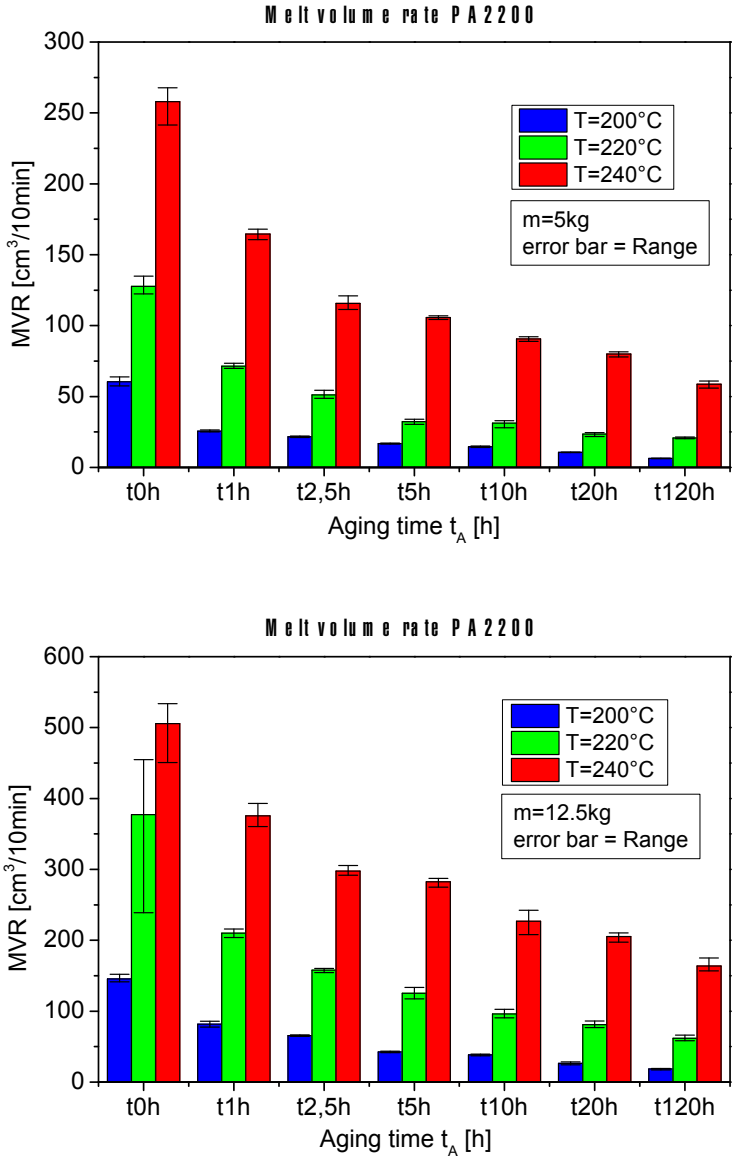

Figure 3: MVR of PA12 (left: m=5kg; right: m=12.5kg)

MVR results at loads of 5kg and 12.5kg (figure 3) show qualitatively comparable behaviour as already observed for 3.8kg (figure 2). In comparison to figure 2, MVR values are higher at a higher load as it can be expected. Overall, a significant influence of aging time at evaluated temperatures throughout all MVR data is visible.

4.2. Thermal imaging results

The aim of the thermal imaging measurements performed was to determine the melt temperatures during and after laser exposure as a function of process parameter settings. All measured temperature values are summarised in Table 2. The measured temperature data for the maximum melt temperature show a huge range of values between 228 °C for the lowest and 330 °C for the highest area energy density, showing only small deviations for the same parameter set. Figure 4 shows, that the correlation between maximum melt

temperature and area energy density can be described by a linear relation. Additionally, melt temperature was measured ten seconds after laser exposure resulting in a range between 171 °C and 193 °C. The lowest measured temperatures are almost identical to actual real powder bed temperature, while the machine pyrometer displays a temperature which is about four degrees higher than the real value. Furthermore, results show that for area energy densities of over 0.025 J/mm² melt temperature remains at or above the materials melting point, resulting in a continuation of particle melting also after laser exposure. However, over that energy density level temperature increases only slightly for a further rise of energy input. The results show that area energy density is sufficient to describe a correlation between process parameter settings and melt temperature. These correlations should be used for further analyses in order to correlate process parameter settings with the melt viscosity.

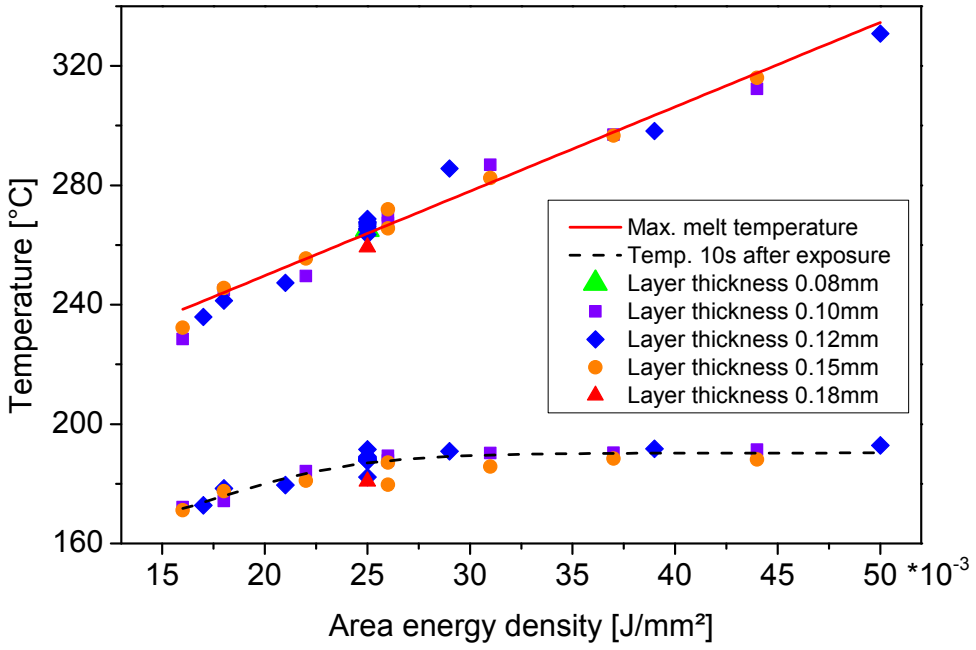

Figure 4: Melt temperatures as a function of area energy density

5. Time and temperature dependent rheological model

In order to make viscosity data useful for the application in a rheological model with shear thinning behaviour, viscosity was corrected according to Giesekus and Langer [33]. This correction provides a true viscosity that was calculated from MVR data for a representative shear rate. Figure 5 shows the true viscosity (subsequent viscosity) as function of aging time in comparison to MVR. The progression of viscosity and MVR is shown exemplarily for a specific temperature and load or shear rate respectively and is representative for other temperature and load combinations which were investigated.

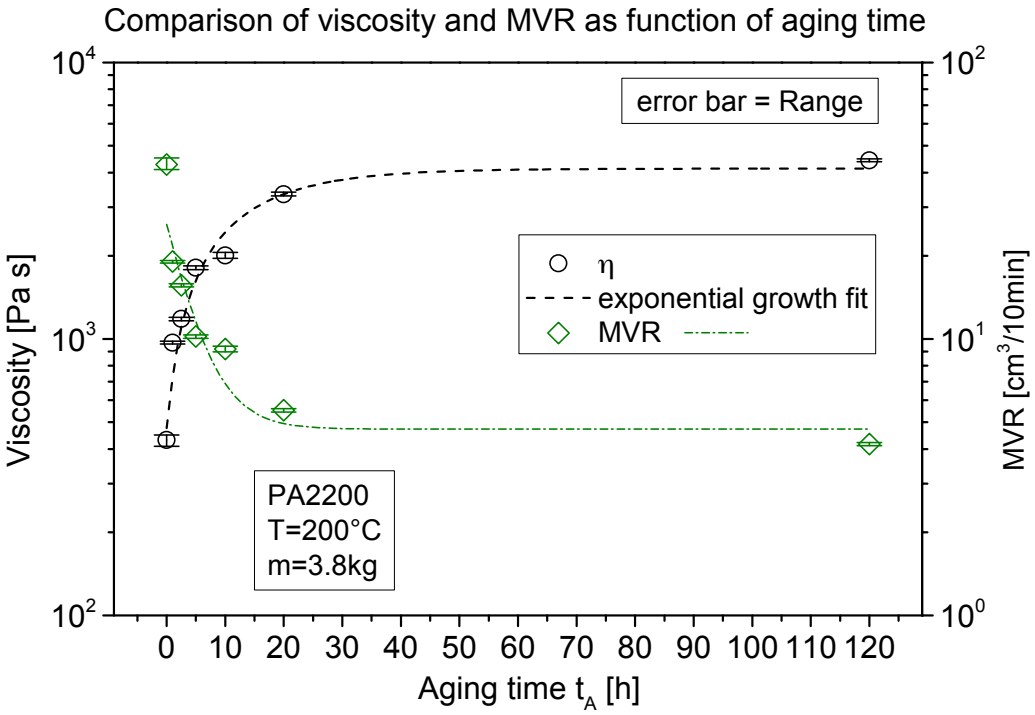

Figure 5: Viscosity and MVR as function of aging time (dashed-dot line is guide to the eye)

The decrease of MVR that has already been described in chapter 2.1 correlates with a significant viscosity build-up as function of aging time, as it can be seen in figure 5. In this example, the average viscosity increases from approx. 431 Pa s to 4425 Pa s after 120h of aging (factor 10.2). Moreover, the viscosity rises significantly fast up to aging times of 20 hours. Further viscosity change is strongly reduced. Within the range of evaluated aging times, the viscosity approaches an upper limit at 120h of aging. The progression of the viscosity build-up follows an exponential behaviour as already implied by the dashed line in figure 5. In fact, an exponential growth model [34] was used to fit the change in viscosity as function of aging time. The application of this model is feasible if viscosity change as result of structural change follows exponential and limited growth behaviour. Applied to viscosity as

function of aging time, the approach can be written as

$$\eta = f(t_A) = \alpha - \beta * \exp(-k * t_A) \quad (1)$$

whereas α > β > 0. The exponential growth model contains 3 parameters. With α [Pa s] the upper viscosity limit, β [Pa s] the initial viscosity and k [1/s] rate of growth or structural change. This approach sufficiently describes the viscosity build-up but is useless in this form for the prediction of viscosity. In fact, figure 5 shows the effect of powder aging time on viscosity where viscosity was measured at 200°C (and at higher temperatures) in liquid (subsequent molten) state on a short time scale but powder was aged at a temperature of 174°C in solid state on a very long time scale. According to the theory of reaction kinetics, a higher temperature will cause a faster structural change (viscosity growth) especially in molten state where kinetic energy is significantly higher. Hence, the description of solid as well as molten state viscosity growth is useful because it corresponds to the LS process. PA12 powder is held in solid state at a powder bed temperature of approx. 174°C for a relatively long time in contrast to the very short time of melt formation and layer-to-layer bonding due to laser exposure and related temperature increase. Here, for the first time thermal imaging measurements provide detailed data about the rate of temperature rise and the melt temperature during and after laser exposure.

With respect to LS process conditions (increased temperature and inert atmosphere), PA12 undergoes a structural change which is observed as significant growth in viscosity (fig.5), concluded as molar mass build-up and understood as post condensation. It is assumed that powder bed temperature leads to molar mass build-up of PA12 because of molecular chain consumption into molecular chain extensions. It is expected further that progressing formation of extended molecular chains however decreases molecular movement and finally freezes post condensation. Viscosity progression shown in figure 5 corresponds to this physiochemical assumption. The consequence for a time and temperature dependent rheological model is expected to be as follows. Molar mass build-up of PA12 will lead to an increase of zero shear viscosity and affect mutual interaction of PA12 macromolecules. As a result, zero shear viscosity as well as transition time, i.e. the time necessary for entanglements to become released resulting in viscous flow due to relative slip of molecular segments will be increased. A rheological model for PA12 with structural change or thermorheological complex behaviour needs to combine the following effects:

1. Shear dependence of viscosity
2. Temperature dependence of viscosity
3. Time and temperature dependence of viscosity due to structural change

5.1. Shear dependence of viscosity

For the consideration of shear dependence, the well-known three parameter Carreau model [35] was used

$$\eta = \frac{\eta_0}{\left[1 + \left(t_1 * \dot{\gamma}\right)^2\right]^{\frac{(1-n)}{2}}} \tag{2}$$

The Carreau model contains three parameters. The characteristic time t_1 [s] corresponds to the transition time between the first Newtonian plateau $\dot{\gamma} \to \infty$ and power law behaviour. The parameter n is the viscosity exponent and is dimensionless. For , the Carreau model also predicts the zero shear viscosity η_0 [Pa s] which is related to the molar mass according to the Mark-Houwink relation [36]

$$\eta_0 = K * \overline{M}_W^{3.4} \tag{3}$$

The Carreau model was used because it is able to predict viscosity within the first Newtonian plateau as well as the transition to power law behaviour. In contrast, the power law of Ostwald- de Waele does not describe the flow behaviour; neither within the transition nor in the first Newtonian region. Up to now, a shear rate or the shear rate range where flow occurs in the unpressurised LS process is still unknown. According to [37] the coalescence of adjacent polymer particles due to flow processes is caused by forces which result from the free surface energy at curved surfaces. It can be assumed that flow occurs at relatively low shear rates and thus within the first Newtonian region predicted by the Carreau model which can also be written in the following form, according to [38]

$$\eta = \frac{A}{\left(1 + B * \dot{\gamma}\right)^C} \tag{4}$$

with A [Pa s] zero shear viscosity (η_0), B [s] transition time and C [-] viscosity exponent or slope.

5.2. Temperature dependence of viscosity

The temperature dependence of the viscosity of PA12 is considered using the temperature shift factor a_T by Arrhenius. The Arrhenius approach is particularly suitable to describe the temperature dependence of viscosity in case of semi-crystalline thermoplastics [39] like PA12. The temperature shift factor a_T can be written as

$$a_T(T,T_0) = \frac{\eta_0(T)}{\eta_0(T_0)} = \exp\left(\frac{E_0}{R} * \left(\frac{1}{T} - \frac{1}{T_0}\right)\right) \quad (5)$$

E_0 is a material dependent flow activation energy [J/mol] and R is the ideal gas constant with R=8,314 J/mol K. If E_0 is determined, a_T is capable to shift the viscosity to a temperature T with respect to the reference temperature T_0. The introduction of the temperature shift factor a_T to the Carreau model yields to

$$\eta\left(T,\dot{\gamma}\right) = \frac{A * a_T(T)}{\left(1 + B * a_T(T) * \dot{\gamma}\right)^C} \quad (6)$$

5.3. Time and temperature dependence of viscosity due to structural change

A combined time and temperature dependence of viscosity is necessary because structural change of PA12 obviously occurs during LS processing conditions. As long as this effect cannot be described correctly, the impact on process and part properties will be unknown. As a result, material quality control as well process control will not be successful and part properties cannot be guaranteed.

As a consequence, a second shift factor a_{SC} (SC: **S**tructural **C**hange) is proposed. It describes the correlation of combined temperature and time influences on the viscosity which is of exponential, limited and according to the experimental results irreversible growth behaviour. The introduction of a_{SC} to equation 6 results in

$$\eta\left(t,T,\dot{\gamma}\right) = \frac{A * a_T(T) * a_{SC}(t,T)}{\left(1 + B * a_T(T) * a_{SC}(t,T) * \dot{\gamma}\right)^C} \quad (7)$$

The viscosity build-up (figure 5) is concluded as a change in molar mass, i.e. molar mass build-up caused by LS process conditions. An effect on zero shear viscosity (A) as well as on transition time is expected. For this reason, the factor a_{SC} is introduced to shift zero shear viscosity (A) as well as transition time (B). For a functional interpretation of a_{SC} several boundary conditions with respect to time dependence are introduced

1. for t = 0 s -> $a_{SC} = 1$
2. for $t \neq 0$ s -> $a_{SC} > 1$
3. for $t \rightarrow \infty$ -> $a_{SC} = a_{SC,UL}$

with a_{SC} [-] structural change shift factor and $a_{SC,UL}$ [-] upper limit of structural change. The time dependence of a_{SC} is described using equation 1 which is valid for an exponential and

limited growth as function of time containing k [1/s] as the rate of growth. Applied to the factor a_{SC} the approach can be written as

$$a_{SC} = f(t) = a_{SC,UL} - \beta * \exp(-k * t) \tag{8}$$

In order to meet the requirement of the first boundary condition, a_{SC} will only become equal to 1 for t = 0 s if $\beta = a_{SC,UL} - 1$. Replacing β with ($a_{SC,UL}$ -1) in equation 8 leads to

$$a_{SC} = f(t) = a_{SC,UL} - (a_{SC,UL} - 1) * \exp(-k * t) \tag{9}$$

This form is already able to describe the time dependence of the shift factor a_{SC} and fulfils boundary conditions 1 to 3. However, the rate of viscosity growth is also temperature dependent and will be described using the Arrhenius equation

$$k = k_0 * \exp\left(-\frac{E_0}{R * T}\right) \tag{10}$$

with k reaction rate constant, k_0 pre exponential factor, E_A [J/mol] activation energy of reaction, R [J/mol K] ideal gas constant and T [K] reaction temperature. Replacing k in equation 9 with equation 10 gives

$$a_{SC} = f(t,T) = a_{SC,UL} - (a_{SC,UL} - 1) * \exp\left(-t * k_0 * \exp\left(-\frac{E_0}{R * T}\right)\right) \tag{11}$$

The consideration of a temperature dependence of the viscosity due to structural change in solid and molten states is accomplished using Time-Temperature-Superposition (TTS), i.e. the effect of solid and molten state is additive. Finally, a_{SC} is given by

$$a_{SC}(t,T) = a_{SC,UL} - (a_{SC,UL} - 1) * \exp\left(\left(-t_A * k_0 * \exp\left(-\frac{E_{0,SC}}{R * T_A}\right)\right) + \left(-t_P * k_0 * \exp\left(-\frac{E_{0,SC}}{R * T_P}\right)\right)\right) \tag{12}$$

and allowing to describe the time and temperature dependence of structural change due to systematic aging of PA12 powder (solid state structural change) as well as MVR study (molten state structural change) with t_A [s] aging time, T_A [K] aging temperature, t_P [s] processing time and T_P [K] processing temperature.

Hence, the time and temperature dependent rheological model for a PA12 can be summarised as follows

$$\eta\left(t,T,\dot{\gamma}\right) = \frac{A * a_T(T) * a_{SC}(t,T)}{\left(1 + B * a_T(T) * a_{SC}(t,T) * \dot{\gamma}\right)^C} \tag{13}$$

with

$$a_T(T) = \exp\left(\frac{E_{0,T}}{R} * \left(\frac{1}{T} - \frac{1}{T_0}\right)\right) \tag{14}$$

and

$$a_{SC}(t,T) = a_{SC,UL} - (a_{SC,UL} - 1) * \exp\left(\left(-t_A * k_0 * \exp\left(-\frac{E_{0,SC}}{R * T_A}\right)\right) + \left(-t_P * k_0 * \exp\left(-\frac{E_{0,SC}}{R * T_P}\right)\right)\right) \tag{15}$$

with the seven parameters

A	[Pa s]	Zero shear viscosity
B	[s]	Transition time
C	[-]	Viscosity exponent
$a_{SC,UL}$	[-]	Upper limit of structural change
k_0	[1/s]	Rate of structural change
$E_{0,T}$	[J/mol]	Flow activation energy
$E_{0,SC}$	[J/mol]	Structural change activation energy

In this particular form (equation 15), a_{SC} considers two different times and temperatures. In a more general form, it can also be written as

$$a_{SC}(t,T) = a_{SC,UL} - (a_{SC,UL} - 1) * \exp\left(-k_0 \sum t_i * \exp\left(-\frac{E_{0,SC}}{R * T_i}\right)\right) \tag{16}$$

with t_i [s], T_i [K] partial time and temperature processes causing structural change.

In fact, this is not the first time that rheological changes due to structural changes are reported and described in a model. Chemorheological models for viscosity prediction of thermosets have already been reported for instance by Chen and Macosko [39] but also can be found in overviews given by [40, 41]. According to [39], viscosity needs to be related to the process conditions as well as to the state of polymerisation and is a function of temperature, conversion and shear rate. This requirement is in agreement with the rheological model presented above as function of temperature, time and shear rate but for a thermoplastic matrix. In comparison to the conversion, the time can be referred to the state of post condensation of PA12.

5.4. Parameter optimisation and comparison of predicted to measured viscosity

Based on the experimental data, the seven parameters of the time and temperature dependent rheological model were optimised using a genetic algorithm. The algorithm was used to optimise the parameters globally according to the least sum of residual squares fit. The result is shown in table 3.

Table 3: Model parameters optimised for a PA12 (PA2200)

Parameter	Unit	Value
A	[Pa s]	329.02
B	[s]	3.16
C	[-]	0.18
$a_{SC,UL}$	[-]	12.67
k_0	[1/s]	5990.65
$E_{0,T}$	[kJ/mol]	105.54
$E_{0,SC}$	[kJ/mol]	71.00

The time and temperature dependence of the shift factor a_{SC} is validated in figure 6 below.

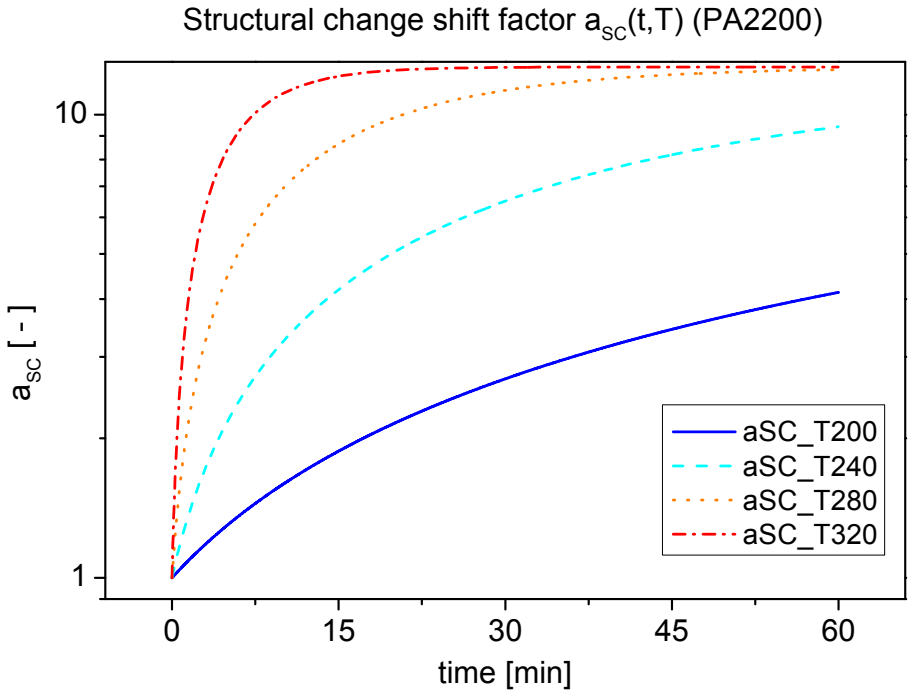

Figure 6: Time and temperature dependence of shift factor a_{SC}

($a_{SC,UL}$=12.67; k_0=5990.65 1/s; $E_{0,SC}$=71.00 kJ/mol; t=0 – 60min)

A significant time and temperature dependence of a_{SC} is clearly visible (figure 6). A higher

temperature causes a faster increase of a_{SC}. The shift factor (fig.6) follows the physiochemical assumption of structural change as result of molar mass build-up or molecular chain extension. a_{SC} describes a limited and irreversible growth behaviour which is a cause of increasing molar mass and reduced molecular movement. However, figure 6 shows a restriction in the use of a_{SC} for viscosity prediction. At a temperature of e.g. 280°C, the rate of structural change is strongly reduced after approx. 30 minutes and is almost at its end after approx. 45 minutes. If PA12 would be exposed to a temperature of 280°C for 45 minutes, molar mass build-up or viscosity growth would be already terminated regarding a_{SC}. Although any further structural change and thus viscosity change cannot be excluded, it cannot be predicted because the parameterisation, especially of $a_{SC,UL}$ forces the structural change to be terminated for $a_{SC,UL}$=12.67. a_{SC} parameters (table 3) were calibrated with respect to LS process related structural change (in solid state) at a temperature of 174°C and measured as MVR or viscosity changes at temperatures of 200, 220 and 240°C. The maximum MVR measuring time (lowest load and temperature, longest aging time) was approx. 15 minutes. As a consequence, the use of a_{SC} for the prediction of viscosity above the melting point of PA12 is only feasible within the times and temperatures of MVR investigation. It is expected that the application of a_{SC} above a temperature of 240°C is valid if time is significantly shorter. Regarding thermal imaging results, it was found that the time within which laser energy is exposed to the powder bed causing temperature raise up to 320°C and melt formation is very short, i.e. $\ll$ 1 minute. Therefore, it can be assumed that the applicability of a_{SC} for viscosity prediction is still allowed.

The shift factor a_{SC} that was calculated for PA2200 at a powder bed temperature of 174°C (in solid state) is shown in figure 7 below. Moreover, the additional effect (in molten state) of MVR measuring temperatures of 200 to 240°C on a_{SC} is presented.

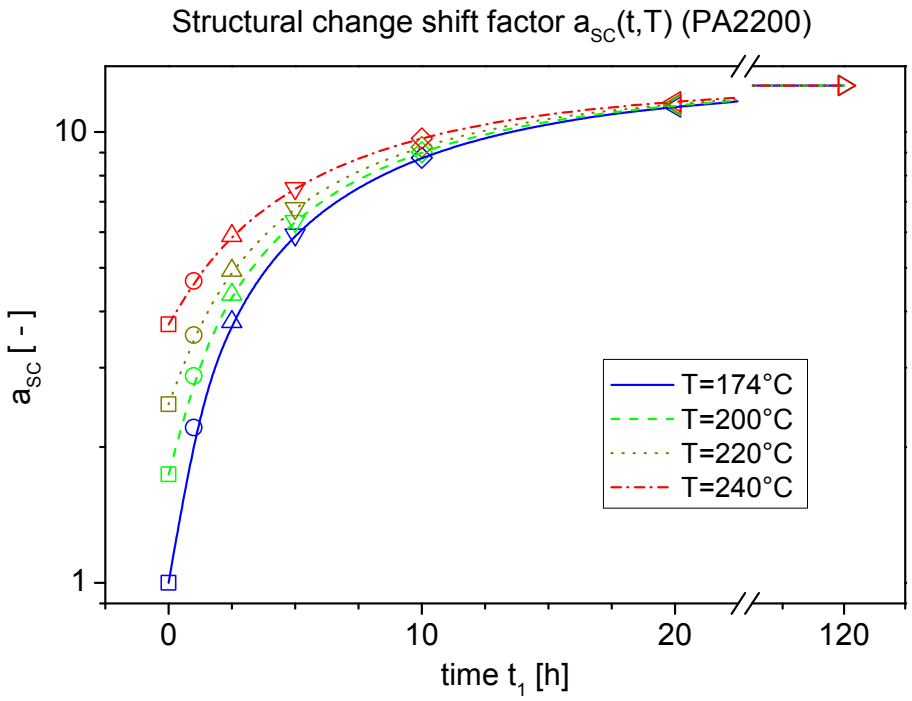

Figure 7: Structural change of PA2200 and additional effect due to MVR measuring time and temperature conditions

($a_{SC,UL}$=12.67; k_0=5990.65 1/s; $E_{0,SC}$=71.00 kJ/mol; t_1=0 – 120h; T_1=174°C, t_2=755.95 s; T_2= 200, 220, 240°C)

For the calculation of a_{SC} according to eq. 16, two time and temperature combination were used. On the one hand the effect of time and temperature due to aging representing index 1. On the other hand the effect of time and temperature during MVR measuring representing index 2. Of course, for t_1=0h the material has not been exposed to a temperature of 174°C. a_{SC} follows the exponential growth behaviour and reaches an upper limit at 120h. The dashed, the dotted and the dashed-dotted lines for temperature of 200 to 240°C show how a_{SC} increases in addition due to measuring conditions. With respect to a best fit of overall MVR data, t_2 = 755.95 s was determined and is approximately in the centre of the shortest and longest times which were necessary in order to obtain MVR data according to the experimental set-up of table 1. Table 4 below summarises tabularly the calculated a_{SC} shift factors of figure 7.

Table 4: a_{SC} shift factors (PA2200)

Aging time	a_{SC}_T=174°C	a_{SC}_T=200°C	a_{SC}_T=220°C	a_{SC}_T=240°C
[h]	[-]	[-]	[-]	[-]
0	1.00	1.74	2.49	3.74
1	2.21	2.87	3.54	4.67
2.5	3.79	4.36	4.93	5.88
5	5.92	6.35	6.78	7.51
10	8.77	9.01	9.26	9.68
20	11.37	11.45	11.53	11.67
120	12.67	12.67	12.67	12.67

Figure 8 (a-c) shows the comparison of predicted (line) to measured viscosity (symbols).

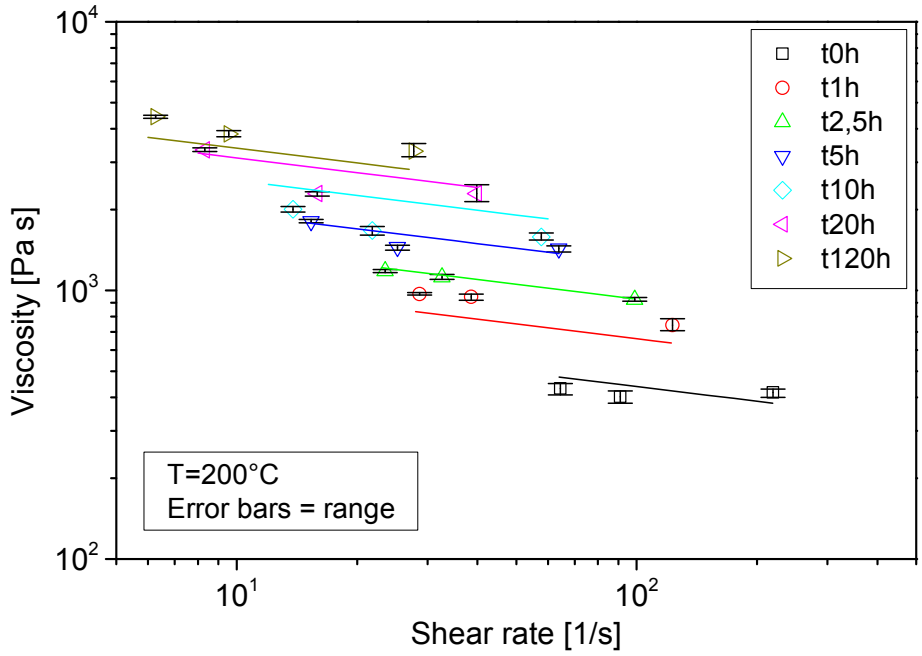

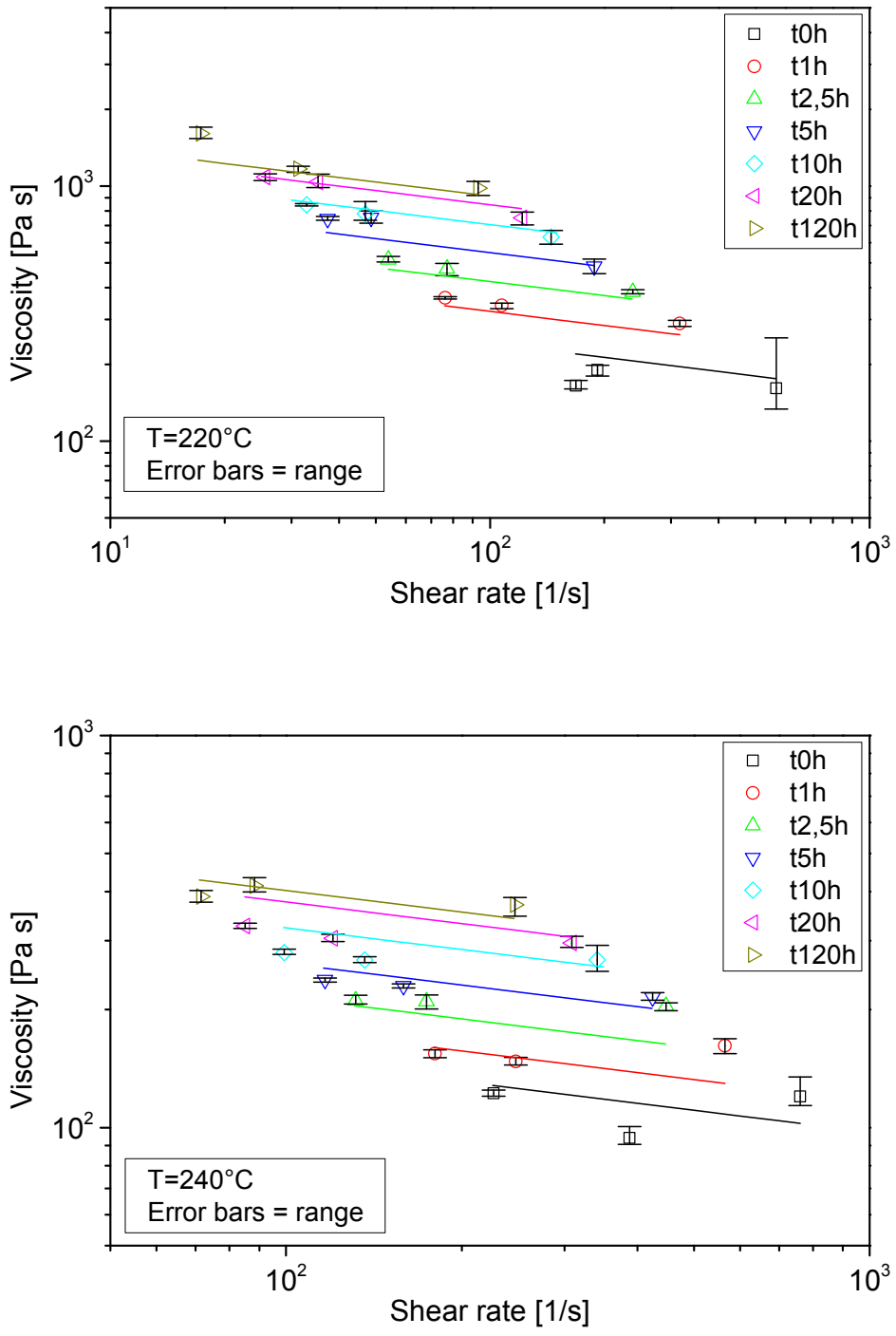

Figure 8: Measured vs. predicted viscosities (a: T=200°C; b: T=220°C; c: T=240°C)

(Symbol = measured viscosity; line = predicted viscosity)

As it can be seen (figure 8 a-c), the comparison of predicted to measured viscosity is found to be in good agreement. Furthermore, the viscosity exponent of 0.18 that was determined using the genetic algorithm is low but reasonable with respect to measured data. Regarding aging time effect described using the structural change shift factor a_{SC}, zero shear viscosity

as well as transition time are increased. This behaviour corresponds to the physiochemical assumption. The shift factor a_{SC} leads to an increase of zero shear viscosity which corresponds to a higher weight average molar mass. In addition, transition time is increased as well and thus shifted towards lower shear rates which is expected if average molar mass is increased.

5.5. Application of the rheological model to LS process data

The time and temperature dependent rheological model was used to predict the viscosity during the laser sintering process as a function of area energy density. The data measured by thermal imaging were used to establish that correlation. Firstly, viscosity was calculated at the maximum melt temperature during laser exposure basing on the determined time and temperature history (figure 9a). Secondly, the same calculation was performed for the temperature, 10 seconds after laser exposure (figure 9b). Additionally, Figures 9a and 9b describe the effect of aging on the viscosity at maximum melt temperature and at melt temperature 10 seconds after laser exposure. Effects of structural changes in molten state were neglected for the calculation of viscosity values, since a_{SC} numbers aren't affected until the second to fourth digit after the decimal point.

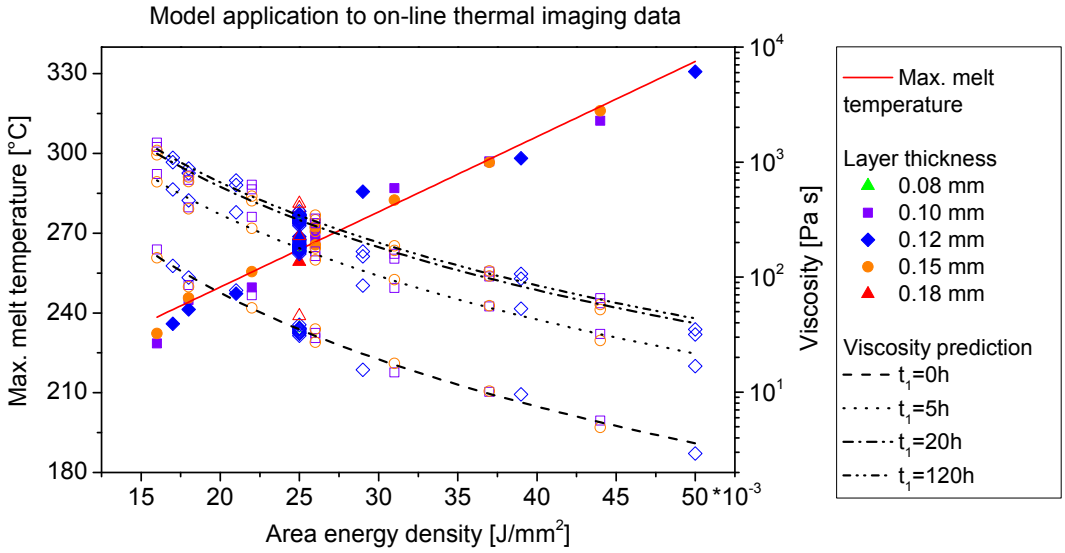

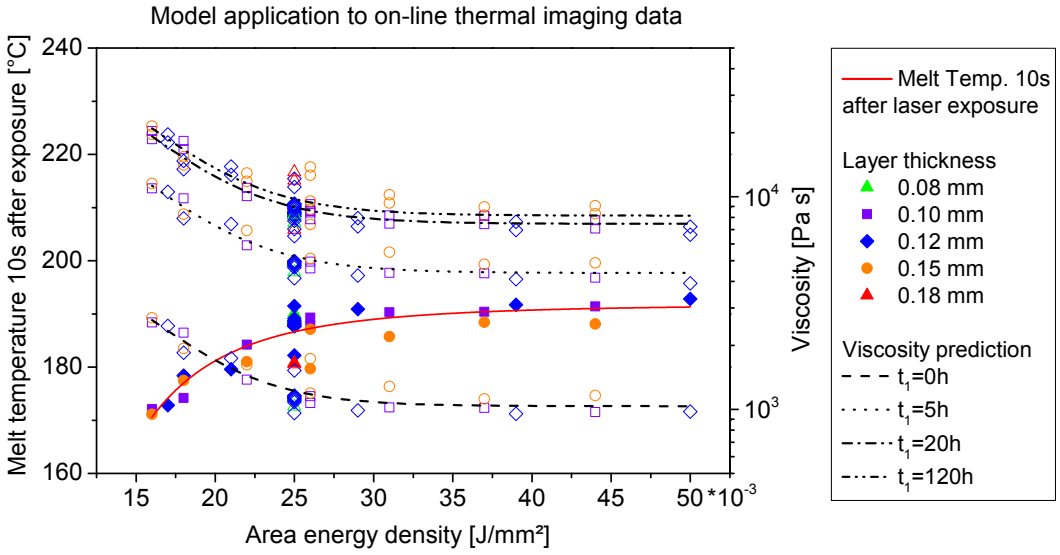

Figure 9: Viscosity predicted for max. melt temperature (a) and for temperature 10s after laser exposure (b) ($\dot{\gamma} = 1\ \ 1/s$; T_0=220°C)

It was found that a higher melt temperature or area energy density respectively decreases the melt viscosity at both temperature levels. However, the viscosity shown in figure 9 a, b significantly increases due to structural change that occurs as a result of time and temperature history of the powder before laser exposure (in solid state), i.e. during long term aging (t= 5, 20, 120h) at relatively low powder bed temperatures (T=174°C). Otherwise, area energy density significantly influences the range between minimum melt viscosities for virgin powder and the maximum values for powder stored 120 h at processing conditions allowing for a partial compensation of aging effects. For the lowest considered energy density of 0.016 J/mm², this maximum difference is about 1208 Pas at maximum melt temperature and about 18300 Pas at the temperature level measured 10 s after laser exposure. An increase in energy density can decrease this range significantly. For an energy density of 0.025 J/mm² these values can be reduced by 75 % and by 54 %, while for 0.037 J/mm² the difference even drops to a level of 10 % and 40 % respectively. These changes in the melt viscosity range will have a significant effect on processing in laser sintering while for the first time giving a correlation between melt viscosity, material aging and process parameter settings. The correlations found show that an increased energy input can compensate effects of powder aging, which was also found by [13] experimentally. Future analysis should validate the results investigated by experimental analysis in order to establish limiting values for melt viscosity as a function of energy density.

6. Conclusion

Long-term aging at temperature of 174°C caused a structural change of PA12, observed as significant viscosity build-up and concluded as change in molar mass, i.e. molar mass build-up caused by LS process conditions. A rheological model that was derived from experimental data is capable to predict the viscosity of a PA12 (PA2200) as a function of time and temperature by means of an additional shift factor a_{SC} which describes the LS process related structural change. The use of a_{SC} parameters, i.e. the rate of structural change k_0, the upper limit $a_{SC,UL}$ and the structural change activation energy $E_{0,SC}$ is valid for viscosity prediction of PA12 within the times and temperatures of MVR investigation. The prediction of PA12 melt viscosity at higher temperatures is only allowed if time is significantly shorter. It is assumed that the rate of structural change as well as the structural change activation energy will differ from the parameter values that were determined based on the LS process related structural change. A prediction of long-term rheological changes above the melting point of PA12 using the structural change shift factor is feasible after a new calibration of $a_{SC,UL}$, k_0 and $E_{0,SC}$.

The rheological model presented can be used to calculate and to control PA12 material quality. If PA12 material quality was found to be out of a tolerable quality range representatively predicted as viscosity, LS process parameters can be adopted systematically or in a process model that correlates material to process and part properties in order to meet the requirement of a quality assured or a model-based quality assured series production. Moreover, viscosity of powder mixtures with different state of post condensation can be calculated in order to determine the required amount of refreshing or in other words to adjust a desired viscosity or processability of the material. Furthermore, the model can be used to study the effects of viscosity changes on sinter kinetics in theory.

Based on viscosity prediction at LS process conditions obtained via thermal imaging, it can be concluded that coalescence of adjacent polymer particles is mainly affected by the time and temperature history prior to laser exposure. These results show as well that a viscosity build-up can be partially compensated by a higher area energy density or higher melt temperature respectively. The study of significant process parameters is important for the identification of a robust process window and process parameters which can be used for quality control and thus for quality assurance.

Further investigations will focus on the processing of systematically aged powders in order to correlate material with process and part properties.

7. Acknowledgements

The authors would like to thank the German Research Foundation DFG for funding the research within the project “Fundamentals for a Quality Assurance System applied to Rapid Manufacturing Processes”.

8. References

[1] Abele, E.: „Herausforderungen für die Produktion(sforschung) 2020“, Presentation on the 10th Karlsruher Arbeitsgespräche Produktionsforschung 2010. Karlsruhe, BMBF.

[2] Hague, R.; et al.: “Implications on design of rapid manufacturing”, Journal of Mechanical Engineering Science, 217 (2003) 1, pp.25-30.

[3] N., N.: Additive fabrication – Rapid technologies (rapid prototyping) – Fundamentals, terms and definitions, quality parameters, supply agreements, VDI-Guideline 3404, Association of German Engineers, 2009.

[4] Gebhardt, A.: Generative Fertigungsverfahren – Rapid Prototyping – Rapid Tooling – Rapid Manufacturing, 3. Edition, Munich, Hanser Publishing, 2007.

[5] Alscher, G.: Das Verhalten teilkristalliner Thermoplaste beim Lasersintern, PhD thesis, Universität-GH Essen, 2011.

[6] Wegner, A., Witt, G.: Process monitoring in laser sintering using thermal imaging. In: Bourell, D.: Proceedings of the 22nd Annual International Solid Freeform Fabrication Symposium: Austin, Texas 2011, pp. 405-414.

[7] Zarringhalam, H.: Investigation into Crystallinity and Degree of Particle Melt in Selective Laser Sintering, PhD thesis, Loughborough University, 2007.

[8] Dotchev, K.; Yusoff, W.: Recycling of polyamide 12 based powders in the laser sintering process, In: Rapid Prototyping Journal, 15 (2009) 3, pp. 192 - 203.

[9] Haworth, B.; Hopkinson, N.; Hitt, D.; Zhong, X.: Shear viscosity measurements on Polyamide-12 Polymers for Laser Sintering, Rapid Prototyping Journal, Vol. 19 Iss: 1 (2012).

[10] Drummer, D.; Kühnlein, F.; Rietzel, D.; Hülder, G.: Untersuchung der Materialalterung bei Pulverbasierten Schichtbauverfahren. In: RTejournal, 8 (2011).

[11] Wortberg, J.: Qualitätssicherung in der Kunststoffverarbeitung: Rohstoff-, Prozeß- und Produktqualität, Hanser, München, 1996.

[12] Pham, D. T.; Dotchev, K. D.; Yusoff, W. A. Y.: Detoriation of polyamide powder properties in the laser sintering process, In: Proceedings of the Institution of Mechanical Engineers Part C – Journal of mechanical engineering science, 222 (2008) 11, pp. 2163-2176.

[13] Wegner, A.; Witt, G.: Betrachtung zur Pulvernutzungsdauer beim Laser-Sintern und Einfluss der Prozessführung auf die Entstehung von Ausschussbauteilen. RTeJournal, 9 (2012).

[14] Choren, J.; Gervasi, V.; Herman, T.; Kamara, S.; Mitchell, J.: SLS powder life study, In: Bourell. D. (Hrsg.): Proceedings of the 12th International Solid freeform fabrication symposium 2001, Austin, Texas, pp. 39 – 45.

[15] Sauer, A.: Optimierung der Bauteileigenschaften beim Selektiven Lasersintern von Thermoplasten, PhD thesis, University of Duisburg-Essen, 2005.

[16] Gornet, T. J.: Materials and process control for rapid manufacturing, In: Hopkinson, N.; et al. (Hrsg.): Rapid Manufacturing - An industrial revolution for the digital age,

Weinheim, Wiley Verlag, 2006, pp. 125-146.

[17] Gornet, T.J.; Davis, K.R.; Starr, T.L.; Mulloy, K.M.: Characterization of selective laser sintering materials to determine process stability. In: Bourell, D. (Hrsg.): Proceedings of the 13th International Solid freeform fabrication symposium 2002, Austin, Texas, pp. 546 - 553.

[18] Seul, T.: Ansätze zur Werkstoffoptimierung beim Lasersintern durch Charakterisierung und Modifizierung grenzflächenenergetischer Phänomene, PhD thesis, RWTH Aachen, 2004.

[19] Pham, D. T.; Dotchev, K. D.; Yusoff, W. A. Y.: Detoriation of polyamide powder properties in the laser sintering process, In: Proceedings of the Institution of Mechanical Engineers Part C – Journal of mechanical engineering science, 222 (2008) 11, pp. 2163-2176.

[20] Pham, D.T.; Dotchev, K.D.; Yusoff, W.A.Y.: Improvement of part surface finishing in laser sintering by experimental design optimization (DOE), In: Pham, D. T.; et. al.: Proceedings of Third Virtual Interanational Conference on Innovative Production Machines and Systems (IPROMS 2007), CRC Press 2007.

[21] Keller, B.: Rapid Prototyping: Grundlagen zum selektiven Lasersintern von Polymerpulver, PhD thesis, University of Stuttgart, 1998.

[22] Nöken, S.: Technologie des Selektiven Lasersinterns von Thermoplasten, PhD thesis, RWTH Aachen, 1997.

[23] Diller, T.; Sreenivasan, R.; Beaman, J.; Bourell, D.; LaRocco, J.: Thermal model of the build environment for polyamide powder selective laser sintering, In: Bourell, D. (Hrsg.): Proceedings of the 21st Annual International Solid Freeform Fabrication Symposium (SSF 2010): The University of Texas at Austin 2010, pp. 539-548.

[24] Fischer, P.; Locher, M.; Romano, V.; et al. (2004). Temperature Measurements during Selective Laser Sintering of Titanium Powder, In: International Journal of Machine Tools & Manufacture, 44 (2004) pp. 1293-1296

[25] Kosolov, S.; Boillat, E.; Glardon, R.; Fischer, P.; Locher, M.: 3D FE simulation for temperaturer evolution in the selective laser sintering process, In: International Journal of Machine Tools & Manufacture, 44 (2004), pp. 117–123.

[26] Wiria, F. E.; Leong, K. F.; Chua, C. K.: Modeling of powder particle heat transfer process in selective laser sintering for fabricating tissue engineering scaffolds, In: Rapid Prototyping Journal, 16 (2010) 6, pp. 400-410.

[27] Kruth, J.P.; Mercelis, P.; Van Vaerenbergh, J.; Craeghs, T.: Feedback control of selective laser melting; In: Bartolo, P. J. et al. (editor): Virtual and Rapid Manufacturing - Advanced Research in Virtual and Rapid Prototyping: Taylor and Francis 2007, pp. 521-527.

[28] Craeghs, T.; Bechmann, F.; Berumen, S.; Kruth, J.-P.: Feedback control of Layerwise Laser Melting using optical sensors, In: Physics Procedia, 5 (2010), pp. 505-514.

[29] Chivel, Y.; Smurov, I.: On-line temperature monitoring in selctive laser sintering/ melting, In: Physics Procedia, 5 (2010), pp. 515-521.

[30] Gao, Y.; Xing, J.; Zhang, J.; Luo, N.; Zheng, H.: Research on measurement method of selective laser sintering (SLS) transient temperature, In: Optik, 119 (2008), pp. 618-623.

[31] Kumpaty, S. K.; Cottrill, D.; Hollett, A.; Barrett, J.; Kamara, S.: An Experimental Study of Heat Transfer in Selective Laser Sintering Process. In: Proceedings of the 9th International Conference on Engineering Education, San Juan, Puerto Rico 2006.

[32] Menges, G.; Wortberg, J.; Michaeli, W.: Abschätzung der Viskositätsfunktion

über den Schmelzindex, Kunststoffe 68 (1978) 1.

[33] Giesekus, H.; Langer, G.: Die Bestimmung der wahren Fließkurven nicht-newtonscher Flüssigkeiten und plastischer Stoffe mit der Methode der repräsentativen Viskosität , Rheol. Acta 16, 1-22 (1977).

[34] Seber, G.A.F.; Wild, C.J.: Nonlinear Regression, New Jersey, John Wiley & Sons, 2003.

[35] Carreau, P.J.; De Kee, D.C.R.; Chhabra, Raj P.: Rheology of Polymeric Systems, Principles and Applications, Hanser, Munich, 1997.

[36] Macosko, C.W.: Rheology: Principles, Measurements, and Applications, VCH, Ney York, 1994.

[37] Reichstein, H.: Beschreibung und Entwicklung von Polymersinterverfahren, PhD thesis, RWTH Aachen, 1982.

[38] Menges, G.; Haberstroh, E.; Michaeli, W.; Schmachtenberg, E.: Menges Werkstoffkunde Kunststoffe, 6., vollständig überarbeitete Auflage, Hanser, München 2011.

[39] Chen, Y.; Macosko, C.W.: Kinetics and Rheology Characterization During Curing of Dicyanates, J. App. Polym. Sci., Vol. 62, 567-576 (1996).

[40] Halley, P.J.; Mackay, M.E.: Chemorheology of Thermosets – An Overview, Polymer Engineering and Science, Vol. 36, No. 5 (1996).

[41] Roller, M.B.; Rheology of Curing Thermosets: A Review, Polymer Engineering and Science, Vol. 26, No. 6 (1986).

9. Contact

Prof. Dr.–Ing. Johannes Wortberg

University of Duisburg-Essen

Institute of Product Engineering

Engineering Design and Plastics Machinery

Lotharstraße 1

47057 Duisburg

E-Mail: **johannes.wortberg@uni-due.de**

WEB: **http://www.uni-due.de/kkm/**

Prof. Dr.–Ing. habil. Gerd Witt

University of Duisburg-Essen

Institute of Product Engineering

Manufacturing Technology

Lotharstraße 1

47057 Duisburg

E-Mail: **gerd.witt@uni-due.de**

WEB: **http://www.uni-due.de/fertigungstechnik/**

M.Sc. Christoph Mielicki

University of Duisburg-Essen

Institute of Product Engineering
Engineering Design and Plastics Machinery
Lotharstraße 1
47057 Duisburg
E-Mail: **christoph.mielicki@uni-due.de**
WEB: **http://www.uni-due.de/kkm/**

Dipl.-Ing. Andreas Wegner
University of Duisburg-Essen
Institute of Product Engineering
Manufacturing Technology
Lotharstraße 1
47057 Duisburg
E-Mail: **andreas.wegner@uni-due.de**
WEB: **http://www.uni-due.de/fertigungstechnik/**

Dipl.-Ing. Burkhard Gronhoff
University of Duisburg-Essen
Institute of Product Engineering
Engineering Design and Plastics Machinery
Lotharstraße 1
47057 Duisburg
E-Mail: **burkhard.gronhoff@uni-due.de**
WEB: **http://www.uni-due.de/kkm/**